
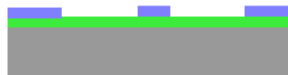





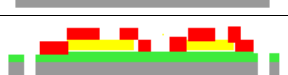


***In Situ* Real Time Monitoring of Surface Transformation : Ellipsometric Microscopy Imaging of Electrografting at Microstructured Gold Surfaces.**

Sorin Munteanu, Nicolas Garraud, Jean Paul Roger, Fabien Amiot, Jian Shi, Yong Chen, Catherine Combellas, Frédéric Kanoufi

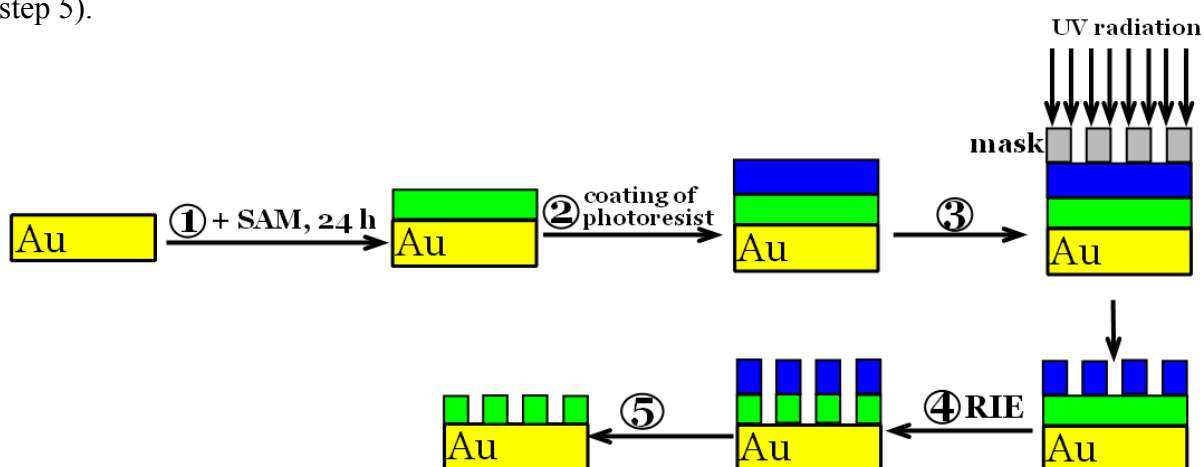
SUPPORTING INFORMATION

1. Materials and methods. 1.1 Materials. 4-Nitrobenzenediazonium (NBD), acetonitrile (ACN), NBu₄BF₄ were used as received from Aldrich. Gold-coated silicon wafers (~1000 Å coating) were purchased from Aldrich and cut into pieces of approximately of ~ 2 x 0.5 cm². Prior to use, the surfaces were ultrasonically rinsed with ethanol and acetone, then cleaned in a bath with H₂SO₄ (conc. 95-98%) to remove the organic residues and finally cleaned with Mili-Q water and dried in a stream of argon. The Au microband arrays were obtained by lithographic procedure detailed below made in FEMTO-ST clean-room facilities, Besançon, France. Below is the flow chart of the process followed to get SU-8 insulated arrays of Au microband electrodes starting from silicon wafers.

| Steps | Schematic structure |
|---|---|
| PECVD silicon nitride deposition on Si |  |
| Coat front side (FS) with resist. Mask the electrode locations. |  |
| Evaporate Cr (5nm) + Au (150 nm) on the FS. Lift-off. |  |
| Coat FS with Al 30 nm by sputtering. |  |
| Unprotected Al is removed by the developer. Coat FS with resist. Mask for the patterns. |  |
| Etch nitride and 300µm Si on the FS with DRIE. |  |
| Etch Al |  |
| Coat FS with 21µm of SU-8 (spray coating). Mask for the insulation layer. |  |

1.2 Grafting of Au samples. The Au surface modification was carried out using 5×10^{-3} M NBD in a solution of ACN containing 0.1 M NaBu_4BF_4 as supporting electrolyte. The solution was degassed for 10 min with argon prior to eletrografting. The surface modification was achieved at a fixed potential, $E = -0.6$ vs Ag/AgCl , for 300 s. After the modification, the sample was rinsed by sonication in ACN, and rinsed in ethanol and acetone, with a final drying under a stream of argon. The surface coating with an organic layer was confirmed by IR analysis or using a conventional ellipsometer. For *in situ* ellipsometry, the grafting of the nitrophenyl layer was carried out in an open cell with typically 5 mL of solution. The grafted samples were then cleaned with ACN, ethanol and acetone and were characterized by conventional ellipsometry and IR analysis

1.3 Patterning of the thiol-SAM layer. A bare gold wafer was immersed for 24 h in a 10^{-3} mol L^{-1} solution of 1-decanethiol (step 1, green rectangle). Then, a photoresist (AZ5214, Clariant) was deposited on the thiolated gold wafer by spin coating (second step, blue rectangle). Here, the spin coating was carried out in 2 steps. The first one was less vigorous to ensure that the Au surface was well covered with the resin (5 s, acceleration: 500 rpm/s, $V = 1500$ rpm). In the second step, the sample was spun at a higher speed (30 s, acceleration: 1000 rpm/s, $V = 4000$ rpm), resulting in a thickness of the photoresist of ~ 1.4 μm . To completely remove the solvent from the photoresist, a baking was performed at 110 $^{\circ}\text{C}$ for 1 min. Afterwards, the photoresist layer was exposed to UV irradiation (365 nm, 100 mJ cm^{-2}) through a mask with the designed pattern (step 3). The photoresist was developed with the AZ726MIF developer (TMAH-tetramethylammonium hydroxide) for 25 s. The final step consisted of reactive ion etching of the exposed thiol layer (RIE, step 4) using O_2 plasma (35 sccm, 100 W, 190 mTorr). Finally, the remaining resin was removed by rinsing the sample in acetone under ultrasound activation, resulting in a pattern of the thiol layer (step 5).



1.4 Ellipsometric Microscopy Imaging

1.4.a Experimental set-up. The optical microscopic version of ellipsometry proposed here is described in Figure S1. An infinity-corrected high-numerical aperture microscope objective is used to achieve angles of incidence large enough to perform sensitive ellipsometric measurements: - a Nikon, 50x, NA=0.95, WD=0.35 mm in air, - an Olympus, 60x, NA=1.1, WD=1.5 mm with an index variation correction collar for observation in liquid. When the light source beam axis is off-centered from the optic axis of the objective, maximum angles of incidence of 54° in air and 45° in a liquid, with a beam divergence of $\pm \sim 2.5^\circ$ can be obtained. The light source is a 637 nm laser diode (Opnext HL6388MG, Thorlabs), with 250 mW CW (continuous wave) optical output power. Its temperature is controlled at 30°C by a thermoelectric cooler element to ensure no deviation of the wavelength from its nominal value (637 nm confirmed spectrophotometrically with spectral bandwidth lower than the 1.5 nm bandwidth allowed by the spectrophotometer).

A rotating diffuser is used to reduce diffraction and interference effects in the image due to the coherence of the laser source. A diaphragm AD, located near the diffuser is conjugated with the back focal plane of the objective. The aperture and angle of incidence of the beam hitting the sample surface are controlled by the diameter and the lateral position of this diaphragm image. A polarizer P, oriented at 45° to the plane of incidence, coupled with a Meadowlark liquid crystal variable retarder (LCVR), with axes parallel to the p and s components produce the state of polarization of the incident wave. This is then analyzed on the second beam transmitted through the non polarizing beam splitter cube BS. The photodiodes D1 and D2 measure the intensities of the components, parallel and perpendicular to the polarizer direction, which are separated by a polarizing beam splitter cube. The D3 photodiode is used to measure the intensity of diffuse light from the laser diode, for normalizing the measured intensities by the photodiodes D1 and D2, in order to compensate the fluctuations of the source.

The measured signals are used for the identification of the phase shifts induced by the LC variable retarder. A calibration is first performed using a Babinet-Soleil compensator as retarder. The Soleil compensator allows creating the initial well-defined polarization states, and the liquid crystal variable retarder is used once the polarimeter has been calibrated. The light collected by the objective passes through an analyzer A parallel to the polarizer P. Finally, the sample surface is imaged onto a CCD array (DALSA, 256x256 pixels, 8 bits). Four images are captured with four different phase shifts of the variable retarder, distributed within the $[0, 360^\circ]$ range ($70, 160, 250, 340^\circ$ for instance) in order to obtain an ellipsometric image.

To improve the sensitivity of the acquisition, we have accumulated 16 images at a frequency of 80 Hz, which corresponds to a total duration of 2.6 s for recording one ellipsometric image. Ellipsometric images are images of the Δ ellipsometric parameter. They may show some residual tilt (residual variation of Δ along the x or y axis). These variations are independent of the nature of the surface. It is corrected from comparison of the recorded image to a reference Δ image taken on bare Au coated wafer surface.

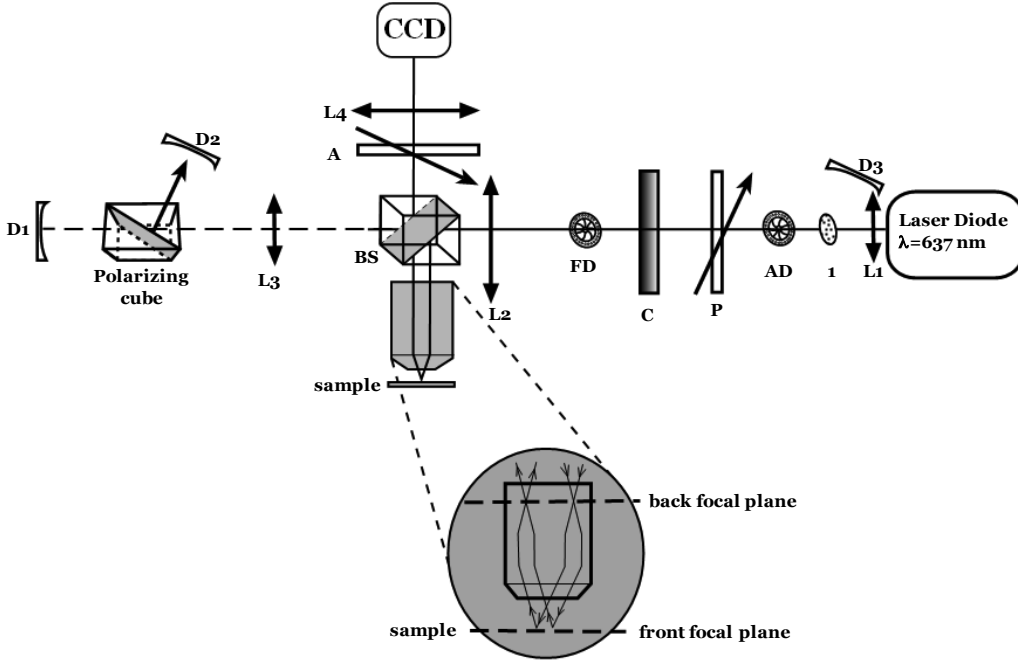


Figure S1. Detailed diagram of the ellipsometric microscope: AD-aperture diaphragm (iris diaphragm); P-polarizer at 45°; C – used as Babinet-Soleil compensator or liquid crystal variable retarder (Meadowlark); FD-field diaphragm; 1- spinning ground glass diffuser; BS – beam splitter; D1, D2,D3 – photodiodes; A – analyzer; L1-L4 – lenses.

1.4.b Image processing

1.4.b.1 *Calibration.* The full system is calibrated introducing N_C well defined phase shifts δ_n^C , $n \in \{1 \dots N_C\}$. Signals $i_{\parallel}^C(n)$, $i_{\perp}^C(n)$, $i_t^C(n)$ coming from the photodiodes are acquired for these shifts as shown in Fig. S2.

The $i_t^C(n)$ is the signal which comes from a third diode, used for the normalization of the signal for the parallel and perpendicular components to the polarizer direction, as in (SI.1). The photodiodes signals are assumed to read:¹

$$\begin{aligned}\frac{i_{\parallel}^C}{i_t^C}(n) &= i_{\parallel}^0 + i_{\parallel}^s \sin \delta_n^C + i_{\parallel}^C \cos \delta_n^C = i_{\parallel}^0 + i_{\parallel}^* \cos(\gamma_{\parallel} + \delta_n^C) \\ \frac{i_{\perp}^C}{i_t^C}(n) &= i_{\perp}^0 + i_{\perp}^s \sin \delta_n^C + i_{\perp}^C \cos \delta_n^C = i_{\perp}^0 - i_{\perp}^* \cos(\gamma_{\perp} + \delta_n^C)\end{aligned}\quad (\text{SI.1})$$

The signals recorded during the calibration procedure are modeled to allow for the identification of the phase shifts induced by the variable retarder. As the imposed phase shifts and the measured signals are known, each Eq. (SI.1) features N_C relationships for only three unknowns ($i_{\parallel}^0, i_{\parallel}^s, i_{\parallel}^C$ for instance). Assuming $N_C > 3$, these two equations systems are thus solved in a least-square sense, to provide the set of unknowns describing the signal measured by each photodiode as a function of the imposed phase shift (Fig. S2). The calibration quality is then assessed through the least-square residual.

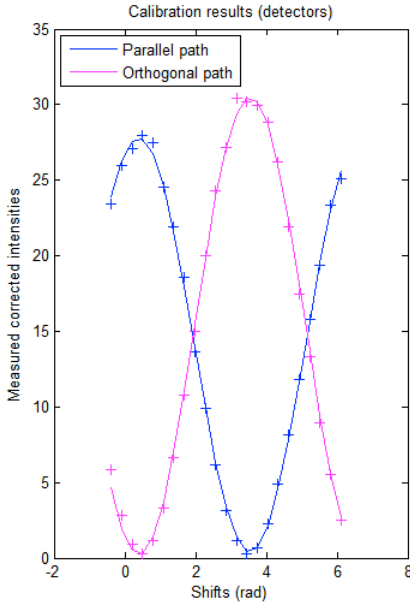


Figure S2. Best fit for measured and normalized intensities (+) for imposed N_C phase shifts values (23, in our case) for the parallel (blue line) and orthogonal (red line) pathes used to obtain $i_{\parallel}^C(n), i_{\perp}^C(n)$ from relation (SI.1).

1.4.b.2 *Image processing: phase shifts identification.* The calibration procedure yields the parameters necessary to identify the actual phase shifts. The latter are computed by using the measured (normalized) photodiodes signals $\frac{i_{\parallel}}{i_t}$ and $\frac{i_{\perp}}{i_t}$ Eqs (SI.1) now read:

$$\begin{aligned}\frac{i_{\parallel}}{i_t} &= i_{\parallel}^0 + i_{\parallel}^* \cos(\gamma_{\parallel} + \delta) \\ \frac{i_{\perp}}{i_t} &= i_{\perp}^0 - i_{\perp}^* \cos(\gamma_{\perp} + \delta)\end{aligned}\quad (\text{SI.2})$$

i_{\parallel}^0 , i_{\perp}^0 , i_{\parallel}^* , i_{\perp}^* , γ_{\parallel} and γ_{\perp} are known from the calibration procedure and δ is the unknown to be determined from the measured normalized photodiodes signals. Denoting \mathbf{i}_m the vector defined by

$$\mathbf{i}_m^t = \left[\frac{i_{\parallel}}{i_t}, \frac{i_{\perp}}{i_t} \right] \text{ and}$$

$$\mathbf{i}_{test}(\delta) = \begin{bmatrix} i_{\parallel}^0 + i_{\parallel}^* \cos(\gamma_{\parallel} + \delta) \\ i_{\perp}^0 - i_{\perp}^* \cos(\gamma_{\perp} + \delta) \end{bmatrix} \quad (\text{SI.3})$$

δ is recovered by as the minimizer of

$$\eta(\delta) = 1 - \frac{\mathbf{i}_m^t \mathbf{i}_{test}(\delta)}{\|\mathbf{i}_m\| \|\mathbf{i}_{test}(\delta)\|} \quad (\text{SI.4})$$

1.4.b.3 Δ field computation

It is obtained from the acquisition of four ellipsometric images, denoted I_1 , I_2 , I_3 and I_4 , captured on the CCD with four phase shifts, δ_1 , δ_2 , δ_3 and δ_4 of the variable retarder. The phase shifts are first recovered using the measured photodiodes signals and the calibration and identification procedure detailed previously. Assuming the polarizers defects vanish, the local intensities measured at pixel P read:¹

$$I_i(P) = I_0(P) + I_s(P) \sin \delta_i + I_c(P) \cos \delta_i \quad \text{for } i \in \{1 \dots 4\} \quad (\text{SI.5})$$

with

$$\begin{aligned}I_0(P) &= A (1 + \tan^2 \Psi(P)) \\ I_s(P) &= -2 A \tan \Psi(P) \sin \Delta(P) \\ I_c(P) &= 2 A \tan \Psi(P) \cos \Delta(P)\end{aligned} \quad (\text{SI.6})$$

For each pixel P , $I_0(P)$, $I_s(P)$ and $I_c(P)$ are first obtained by solving (in a least-square sense) the (over-determined) set of four equations (SI.5). The map for Δ is finally obtained as:

$$\Delta(P) = \tan^{-1} \left(\frac{-I_s(P)}{I_c(P)} \right) \quad (\text{SI.7})$$

1.5 Theoretical variations of the ellipsometric parameters

1.5.a Theoretical sensitivity estimate. It is assumed that a deposited thin organic film can be optically modeled by a simple layer of an homogeneous and isotropic medium of refractive index $n_{\text{film}} = 1.5$, bounded by planar and steep interfaces to a gold reflecting surface, of index n_{Au} , and to

an isotropic ambient medium (air or liquid of $n_A=1$ or 1.33 respectively). The value of $n_{Au} = 0.15 + 3.5i$ was chosen as the mean value (deviation 0.01 and 0.06 respectively for the real and imaginary parts) measured experimentally from spectroscopic ellipsometer (SOPRA ES4G) for Au coated silicon substrates obtained by two different coating methods (chemical vapour deposition and evaporation). The expected variation of Δ with the thickness of the deposited layer can then be calculated by simulation. The evaluation is based on the estimate of the polarized reflectivities r_p and r_s :

$$r_p = \frac{r_p^{AF} + r_p^{FS} e^{iD}}{1 + r_p^{AF} r_p^{FS} e^{iD}} \quad (SI.8)$$

$$r_s = \frac{r_s^{AF} + r_s^{FS} e^{iD}}{1 + r_s^{AF} r_s^{FS} e^{iD}} \quad (SI.9)$$

where r_p^{AF} , r_s^{AF} , r_p^{FS} , r_s^{FS} are the complex Fresnel reflection coefficients of ambient/film and film/substrate interfaces for p and s components.

The complex Fresnel reflection coefficients of ambient/ film (similar for the film/substrate interface) are given by:

$$r_p^{AF} = \frac{n_A / \cos \phi_A - n_{film} / \cos \phi_F}{n_A / \cos \phi_A + n_{film} / \cos \phi_F} \quad (SI.10)$$

$$r_s^{AF} = \frac{n_A \cos \phi_A - n_{film} \cos \phi_F}{n_A \cos \phi_A + n_{film} \cos \phi_F} \quad (SI.11)$$

ϕ_A is the angle of incidence and ϕ_F the angle of refraction in the film.

D is the phase shift due to the travel of light in the film:

$$D = \frac{4\pi}{\lambda} n_{film} d \cos \phi_F \quad (SI.12)$$

d is the deposited film thickness.

Let us recall the basic equation of ellipsometry :

$$\rho = \frac{r_p}{r_s} = \tan \psi e^{i\Delta} \quad (SI.13)$$

where r_p and r_s correspond to complex reflection coefficients of light linearly polarized parallel (p) and perpendicular (s) to the plane of incidence. Δ and $\tan \psi$ are the relative phase and amplitude change respectively, between p and s polarized components due to reflection from the surface.

For reflection from a film-covered surface, the basic equation of ellipsometry (SI.13) becomes:

$$\rho = \frac{(r_p^{AF} + r_p^{FS} e^{iD})(1 + r_s^{AF} r_s^{FS} e^{iD})}{(r_s^{AF} + r_s^{FS} e^{iD})(1 + r_p^{AF} r_p^{FS} e^{iD})} = \tan \psi e^{i\Delta} \quad (\text{SI.14})$$

For given values of the optical constants of the three media involved (ambient, film, substrate), the thickness of the film and the angle of incidence, the ellipsometric parameters ψ and Δ can be computed by use of equation (SI.14).

1.5.b Theoretical variation of Δ in air

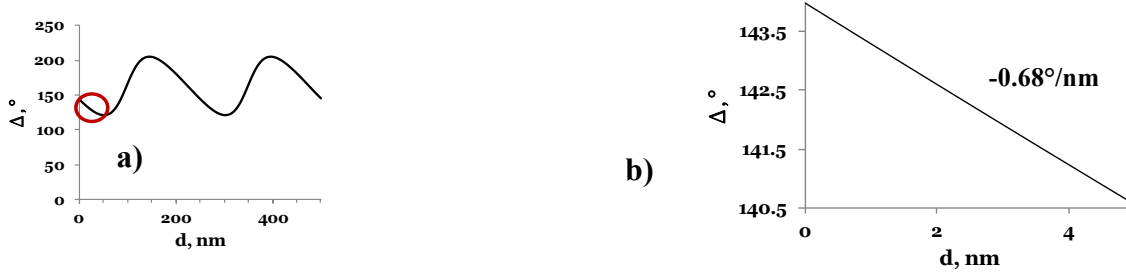


Figure S3. Δ in degrees as a function of deposited organic film thickness d on gold in air; a) Δ variation in degrees for a deposited film of 500 nm; the black line is calculated from the one layer optical model with $\lambda = 637$ nm light, incidence angle = 55° , $n_{\text{Au}} = 0.15 + 3.5i$, $n_{\text{film}} = 1.5$. b) linear region of Δ periodic variation with d (red circle in a).

The predicted variations of Δ with d in air and in a liquid are valid with $< 0.5\%$ change when taking into account possible uncertainties in the refractive index of Au ($n_{\text{Au}} = 0.15 \pm 0.02 + (3.5 \pm 0.1)i$).

1.6. Experimental performances

1.6.a. Limit of detection. Fig S4 presents the standard deviation (STD) in $\delta\Delta$ measured on a bare gold surface in air between 2 final images as a function of the number of accumulations. When the number of accumulations is increased, the STD in each pixel is decreased, while the total time needed for the image acquisition is considerably increased.

Moreover, the STD for $\delta\Delta$ over a sequence of 6 images in Δ (each made from 16 accumulations) is 0.04° in liquid media as well as in air. This value is smaller than the LOD, which means that possible variations of the recorded signal will not affect the measurements.

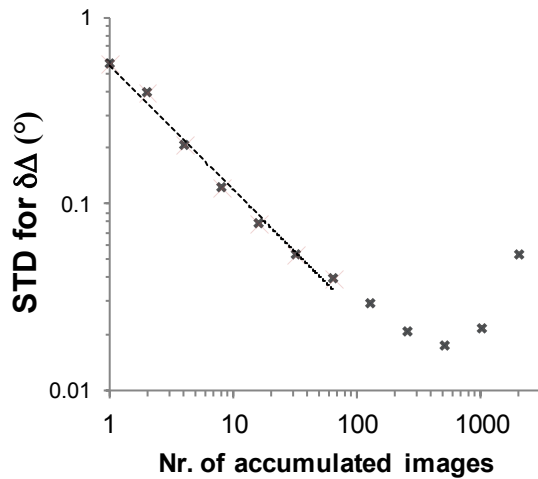


Figure S4. Limit of detection of the ellipsometric microscope deduced from the variation of the standard deviation of $\delta\Delta$ (°) on single pixel with the number of accumulated images.

1.6.b. Lateral resolution. The lateral resolution was estimated through imaging of a diffraction gratings defined by periodic knife edge structures of 7 μm wide Al bands with a 3 μm inter band distance. The given magnification objective, in air, yields a $90 \times 90 \mu\text{m}^2$ imaged zone of the gratings (corresponding to 256×256 pixels, Fig. S5a). A knife edge plot (experimental dots and dashed line) is extracted from this image by pixel by pixel analysis of the normalized light intensity along the axis normal to the edge structure (Fig. S5b). Such knife edge plot obtained by an optical microscopic setup is expected to follow the theoretical spread function given by the edge spread function, ESF, which can be expressed as:²

$$f_{\text{knife-edge}}(x) = \frac{1}{\pi} a \tan\left(\frac{x}{\alpha}\right) + \frac{1}{2} \quad (\text{SI.15})$$

where 2α corresponds to the lateral resolution of the imaging technique.

By fitting the knife edge plot with the ESF function (black line in Fig. S5b), a resolution of $2\alpha=3.25$ pixels is obtained, corresponding to a resolution of 1.2 μm in air. Similarly, in a liquid medium, a resolution of $\sim 1 \mu\text{m}$ is obtained.

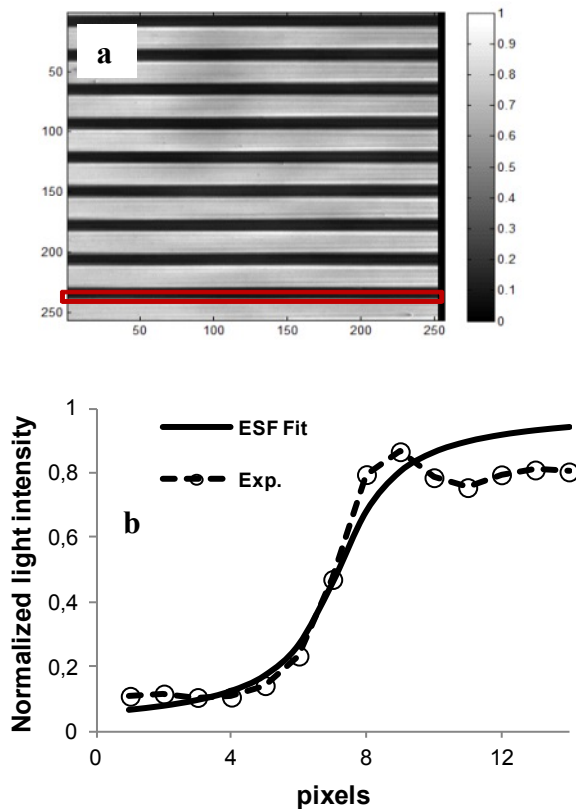


Figure S5. Experimental lateral resolution of the ellipsometric microscope from a) image of a diffraction gratings and b) Cauchy fit of one of its knife edge structure (red rectangle in a).

2. Illustration of ellipsometric imagery in liquid medium of ex-situ modified surfaces

2.1. Centimeter large surface. The imaging capability in a liquid solution was inspected. This is shown first from the imaging of interfacial electrografted regions. An image taken in liquid is presented in Figure S6. It provides observations similar to those obtained from Figure 3 taken in the air.

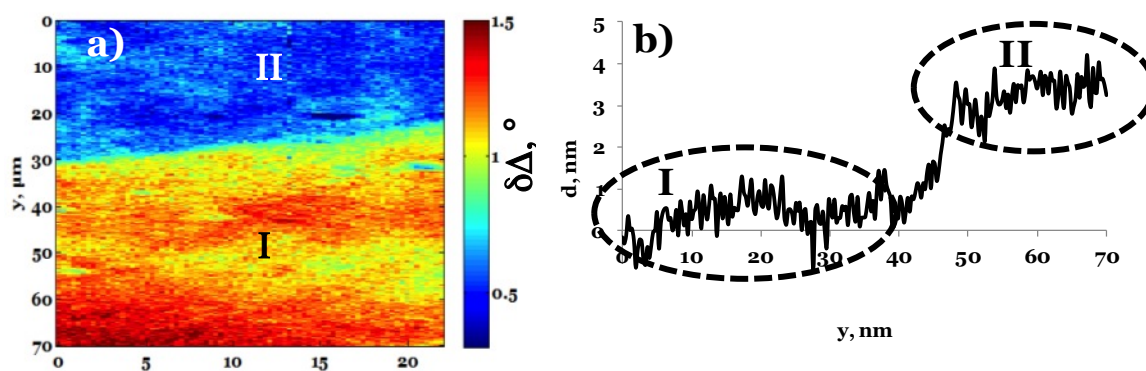


Figure S6. a) Image border of an *ex situ* grafted nitrophenyl film on gold with a thickness of ~ 4 nm in a liquid; b) Structure of film border (profile on 'y' direction).

The limit between grafted and bare gold (I, red-yellow – bare Au; II, blue – grafted region) can be easily distinguished in the image a) or on the profile b) of the deposited film thickness along the 'y' direction. The conversion of the $\delta\Delta$ variations into layer thickness with the estimated sensitivity in liquid (-0.2° /nm of deposited organic layer, $n=1.5$) is also consistent with a 4 nm thick layer obtained with a conventional ellipsometer. This illustrates the trueness of the measurement provided by this ellipsometric microscope in a liquid.

2.2. Microfabricated surfaces. Figure S7 presents the ellipsometric image of an array of microbands (7 μm wide Au bands spaced by 3 μm Si_3N_4 interbands) submitted to vigorous electrografting in an ACN solution of NBD + 0.1 M NBuBF_4 . This *ex situ* grafted substrate was then rinsed and observed by the ellipsometric imaging microscope in an ACN liquid medium. Vigorous electrografting was performed to enforce the deposition of a thick organic layer on the electrically connected microbands (n° 1, 2, 6 and 7). The other microbands (n° 3, 4 and 5) and the

Si₃N₄ interbands were unconnected. This was achieved from electrografting of NBD under a highly reductive potential ($E = -1.2\text{V}$ vs Ag/AgCl).^{3,4}

The microbands are characterized as regions of low Δ values in Figure S7a and the Si₃N₄ interbands as dark red regions. The high heterogeneity in Δ values observed on the connected Au bands indicates the poor optical quality of the organic deposition under such highly reductive potential. Owing to the theoretical periodic variations of the ellipsometric signal with the film thickness, it is not possible to determine the coating thickness from this image and *in situ* real time monitoring would have been preferred for growth kinetic investigation. However, pertinent information may be gathered from such image. Despite the high heterogeneity of Δ over the connected Au bands, revealing the high coating heterogeneity, the grafted bands are characterized by regions of Δ higher than those recorded on unconnected bands. From the theoretical prediction plotted in Fig 2, it suggests that the deposited film may be locally thicker than 150 nm. Moreover, the $\delta\Delta$ between grafted and non-grafted bands may reach up to 25° exceeding the theoretical maximum variation indicating that the optical modelling of thick multilayers should be refined. Under the highly reductive conditions used during the electrografting of Figure S7a, the anion radical of nitrobenzene is also generated at the connected Au microbands. Such a stable anion radical was already ascertained to explain the growth of thick μm layers from diazonium bearing electroactive moieties (anthraquinone, NP), as confirmed here.

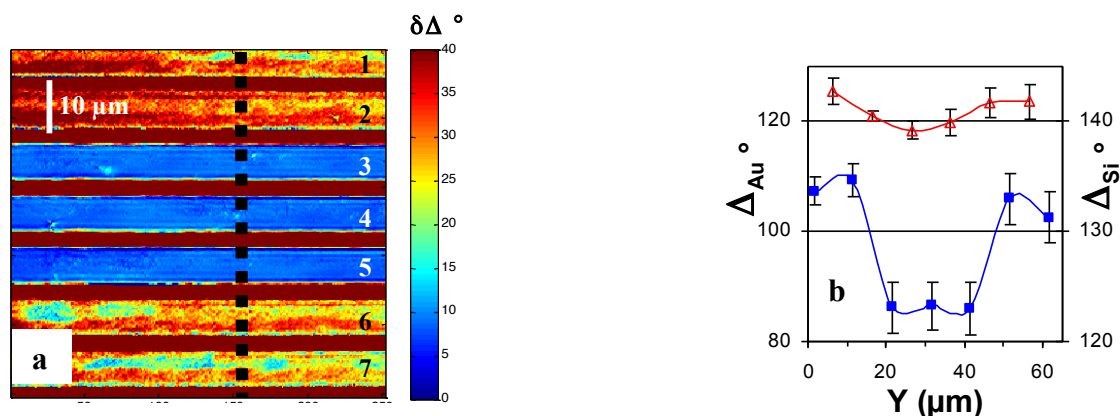


Figure S7. *Ex situ* ellipsometric imaging of an Au micro-electrode array electrografted with NBD. a) $\delta\Delta$ ($^\circ$) distribution image showing the grafted microbands as regions of lower $\delta\Delta$ values; b) average Δ on individual patterns (Au in blue or Si) along the 'y' direction (dashed line in a).

¹ a) Azzam R. M. A.; Bashara, N. M. In *Ellipsometry and Polarized Light*, North-Holland, **1987**. b) Acher, O.; Bigan, E.; Drévilion, B. *Rev. Sci. Instrum.* **1989**, *60*, 65-77.

² Barney Smith E.H. *Proc. SPIE 6059*, Image Quality and System Performance III, **2006**, doi:10.1117/12.643071.

³ Bureau, C.; Levy, P.; Viel, E. *PCT Int. Appl.* **2003**, WO 03018212.

⁴ a) Ceccato, M.; Bousquet, A.; Hinge, M.; Pedersen, S.U.; Daasbjerg, K. *Chem. Mater.* **2011**, 23, 1551-1557. b) Bousquet, A.; Ceccato, M.; Hinge, M.; Pedersen, S.U.; Daasbjerg, K. *Langmuir* **2012**, 28, 1267-1275.